Tomographic measurement of the density matrix of the radiation field

G M D'Ariano

Dipartimento di Fisica 'A Volta', via Bassi 6, I-27100 Pavia, Italy

Abstract. Recently a novel homodine tomographic technique has been proposed which allows us to detect the density matrix experimentally in terms of averages on data. The method has been further extended to a general matrix element $\langle\psi|\hat{\varrho}|\varphi\rangle$ of the density operator $\hat{\varrho}$, along with the possibility of using low-efficiency detectors. In this paper this technique is reconsidered as a new genuine quantum measurement. Numerical results for measured probabilities are given, and the mechanism underlying the generation of statistical errors in the measured matrix is illustrated. It is shown that the data processing of the novel technique can also be used as a new imaging algorithm for conventional tomography.

1. Introduction

In quantum optics, differently from the quantum mechanics of particles, one has the unique opportunity of measuring all possible linear combinations of position $\hat{q}$ and momentum $\hat{p}$ of the oscillator field mode a. This can be achieved by means of a balanced homodyne detector, which measures the quadrature $\hat{x}_\phi = \frac{1}{2}(a^\dagger e^{i\phi} + a e^{-i\phi})$ at any desired phase ϕ with respect to the local oscillator. The homodyne-tomography technique originated from the idea that the collection of probability distributions $\{p(x,\phi)\}_{\phi\in[0,\pi)}$ is just the Radon transform (or 'tomography') of the Wigner function $W(\alpha,\bar{\alpha})$ [1]. By inverting the Radon transform one can obtain $W(\alpha,\bar{\alpha})$ from $p(x,\phi)$ and then from $W(\alpha,\bar{\alpha})$ one recovers the matrix elements of the density operator $\hat{\varrho}$. This is the basis of the method proposed by Smithey *et al* [2] to detect the density matrix experimentally. However, the inversion of the Radon transform needs *analytic* knowledge of $p(x,\phi)$, and hence, strictly speaking, this method is not a measurement of the density matrix. In fact, the inverse Radon transform is achieved by 'filtering' data, as in the usual x-ray medical tomography, and a suitable cut-off is required which sets the resolution for $W(\alpha,\bar{\alpha})$. The data filtering is equivalent to a set of assumptions on the quantum state (in the end it is just a 'fit' on *a priori* analytic forms for $p(x,\phi)$). Moreover, setting the resolution for $W(\alpha,\bar{\alpha})$ in advance makes the state 'more classical', thus losing the most interesting features which the experimentalist is looking for.

In [3] D'Ariano *et al* presented a new technique which provides the matrix elements in the number representation simply in terms of averages on data, avoiding the evaluation of $W(\alpha,\bar{\alpha})$ as an intermediate step. In this paper I will show that this method actually corresponds to a genuine measurement of the density matrix. More recently, D'Ariano *et al* [4] addressed the problem of experimentally 'sampling' a general matrix element $\langle\psi|\hat{\varrho}|\varphi\rangle$. They also showed that experimental sampling is also possible for non-unit efficiency η at the detectors, provided that η satisfies a lower bound related to the 'resolutions' of vectors $|\psi\rangle$ and $|\varphi\rangle$ in the quadrature representations. Hence,

not all matrix representations can be measured, nor are 'experimentally equivalent': however, for coherent and number-state representations the matrix can be measured for $\eta > \frac{1}{2}$.

In this paper the homodyne-tomography technique of [3,4] will be reconsidered as a new type of genuine quantum measurement. Part of section 2 (from equation (3)) and sections 3 and 4 are a short review of [4]). In section 5 I will describe the mechanism underlying the generation of statistical errors in the measured matrix, showing that non-unit efficiency produces errors that dramatically increase for large numbers of photons in the matrix indices. Numerical results will be given for the tomographically measured number probability. In section 6 I will give samples of a tomographic reconstruction of the Wigner function from the measured matrix elements. In section 7 I will briefly explain how the 'data processing' algorithm of the present method can also be used as a new tool for conventional tomographic imaging and for image compression: more details on this topic will be available in a forthcoming paper with Macchiavello and Paris. Finally, section 8 concludes the paper with a summary of the most relevant results.

2. Basis of the method

A homodyne tomography of a single mode a of the field is an ensemble of repeated measurements of the quadratures $\hat{x}_\phi = \frac{1}{2}\left(a^\dagger e^{i\phi} + a e^{-i\phi}\right)$ scanning the phase $\phi \in [0, \pi)$ relative to the local oscillator. The quadrature $\hat{x}_\phi$ is measured by means of a balanced homodyne detector (see figure 1).

The aim is to measure a matrix element $\langle\psi|\hat{\varrho}|\varphi\rangle$ between vectors ψ and φ from the random outcomes x of $\hat{x}_\phi$. Strictly speaking, by 'measurement' I mean the following sequence of actions:

(i) *Collecting data*: get many outcomes x of $\hat{x}_\phi$ with $\phi \in [0, \pi)$.
(ii) *Processing data*: evaluate functions $x \rightarrow f_{\psi\varphi}(x, \phi)$ whose (theoretically given) analytic form depends parametrically on the vectors ψ and φ.
(iii) *Averaging data* over x and ϕ: $f_{\psi\varphi}(x, \phi) \rightarrow \overline{f_{\psi\varphi}(x, \phi)} \equiv \langle\psi|\hat{\varrho}|\varphi\rangle$. (In the following theoretical and experimental expected values are identified by the same symbol.) In terms of the probability densities $p(x, \phi)$ the average of a function f is given by

$$\overline{f(x, \phi)} = \int_0^\pi \frac{\mathrm{d}\phi}{\pi} \int_{-\infty}^{+\infty} \mathrm{d}x \, p(x, \phi) f(x, \phi). \tag{1}$$

The averaged function $f_{\psi\varphi}$ will also be referred to as the 'kernel' or 'data processing' rule.
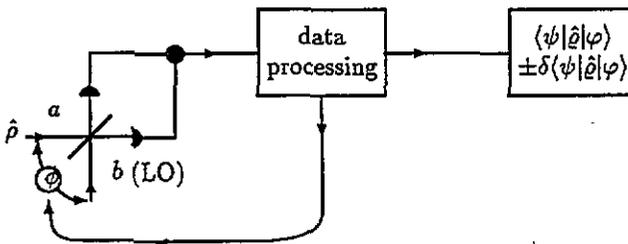
Figure 1. Scheme of tomographic detection of the density matrix $\langle\psi|\hat{\varrho}|\varphi\rangle$.

(iv) *Evaluating errors*: confidence intervals $\delta\langle\psi|\hat{\varrho}|\varphi\rangle$ are obtained according to the central-limit theorem.

Notice that the above operational definition of measurement does not include any kind of smoothing or best fit. The resulting outline of the experimental set-up is sketched in figure 1.

The previous definition of measurement leads to the following general rule:

- the matrix element $\langle\psi|\hat{\varrho}|\varphi\rangle$ can be measured if and only if the kernel $f_{\psi\varphi}(x,\phi)$ is bounded versus x and ϕ.

Boundness of the kernel guarantees that every kernel moment is also bounded for all possible (*a priori* unknown) probability densities $p(x,\phi)$. Then, according to the central-limit theorem one has that:

(i) the matrix element can be sampled on a sufficiently large set of data;
(ii) the average values for different experiments will be normal-Gaussian distributed around the 'true' value, allowing estimation of confidence intervals ('errors').

Now we can readily see that the Wigner function cannot be measured by optical homodyne tomography. In fact, the Wigner function is defined as

$$W(\alpha,\bar{\alpha}) = \int \frac{\mathrm{d}^2\lambda}{\pi^2} e^{\alpha\bar{\lambda}-\bar{\alpha}\lambda}\mathrm{Tr}\left(\hat{\varrho}\, e^{\lambda a^\dagger - \bar{\lambda}a}\right) \tag{2}$$

and changing to polar variables $\lambda = (\mathrm{i}/2)re^{\mathrm{i}\phi}$ and evaluating the trace on the eigenvectors $\{|x_\phi\rangle\}$ of $\hat{x}_\phi$, we obtain

$$W(\alpha,\bar{\alpha}) = \int_{-\infty}^{+\infty} \frac{\mathrm{d}r|r|}{4} \int_0^\pi \frac{\mathrm{d}\phi}{\pi} \int_{-\infty}^{+\infty} \mathrm{d}x\, p(x,\phi)\exp\left[\mathrm{i}r(x-\alpha_\phi)\right] \tag{3}$$

with $\alpha_\phi = \mathrm{Re}(\alpha e^{-\mathrm{i}\phi})$. Equation (3) just states that $W(\alpha,\bar{\alpha})$ is the inverse Radon transform ('back projection') of $p(x,\phi)$. Now we write (3) in the sampling form (1) by exchanging integrals over ϕ and x with respect to the outer integral over r. We have

$$W(\alpha,\bar{\alpha}) = \int_0^\pi \frac{\mathrm{d}\phi}{\pi} \int_{-\infty}^{+\infty} \mathrm{d}x\, p(x,\phi)\, K(x-\alpha_\phi) \tag{4}$$

where the kernel $K(x)$ is given by

$$K(x) = -\frac{1}{2}\mathrm{P}\frac{1}{x^2} \doteq -\lim_{\varepsilon\to 0^+}\frac{1}{2}\mathrm{Re}\frac{1}{(x+\mathrm{i}\varepsilon)^2}. \tag{5}$$

In equation (5) P denotes the Cauchy principal value. From equations (4) and (5) it is clear that $W(\alpha,\bar{\alpha})$ cannot be measured ($\equiv$ statistically sampled), because the kernel $K(x-\alpha_\phi)$ is unbounded as a function of x and ϕ. This is the reason why the method of [2] is not a measurement of $W(\alpha,\bar{\alpha})$ nor of $\langle\psi|\hat{\varrho}|\varphi\rangle$.

In order to obtain the data processing rule for measuring a general matrix element $\langle\psi|\hat{\varrho}|\varphi\rangle$ we seek a sampling formula in the form

$$\langle\psi|\hat{\varrho}|\varphi\rangle = \int_0^\pi \frac{\mathrm{d}\phi}{\pi} \int_{-\infty}^{+\infty} \mathrm{d}x\, p(x,\phi)\, K_{\psi,\varphi}(x,\phi) \equiv \overline{K_{\psi,\varphi}(x,\phi)}. \tag{6}$$

Starting from the operator identity

$$\hat{\varrho} = \int \frac{\mathrm{d}^2\lambda}{\pi} \mathrm{Tr}\left(\hat{\varrho}e^{\lambda a^\dagger - \bar{\lambda}a}\right) e^{\bar{\lambda}a - \lambda a^\dagger} \tag{7}$$

by the same change to polar variables of (3), we obtain

$$\hat{\varrho} = \int_{-\infty}^{+\infty} \frac{\mathrm{d}r|r|}{4} \int_0^\pi \frac{\mathrm{d}\phi}{\pi} \mathrm{Tr}\left(\hat{\varrho}e^{\mathrm{i}r\hat{x}_\phi}\right)e^{-\mathrm{i}r\hat{x}_\phi}. \tag{8}$$

Using the resolution of identity in terms of the eigenvectors $\{|x_\phi\rangle\}$ of $\hat{x}_\phi$ and exchanging integrals we have

$$\hat{\varrho} = \int_0^\pi \frac{d\phi}{\pi} \int_{-\infty}^{+\infty} dx\, p(x, \phi) K(x - \hat{x}_\phi) \tag{9}$$

where again $K(x) = -\frac{1}{2}P\frac{1}{x^2}$. Taking the matrix elements of both sides of (9) we obtain the desired sampling formula

$$\langle \psi|\hat{\varrho}|\varphi\rangle = \int_0^\pi \frac{d\phi}{\pi} \int_{-\infty}^{+\infty} dx\, p(x, \phi)\langle \psi|K(x - \hat{x}_\phi)|\varphi\rangle . \tag{10}$$

The matrix element $\langle \psi|\hat{\varrho}|\varphi\rangle$ can be measured if the kernel $\langle \psi|K(x - \hat{x}_\phi)|\varphi\rangle$ in (10) is bounded as a function of x and ϕ. Notice that the matrix element $\langle \psi|K(x - \hat{x}_\phi)|\varphi\rangle$ can be bounded despite the kernel $K(x)$ not being bounded (as an example, consider the delta-function $\delta(x - \hat{x}_\phi) = |x\rangle_{\phi\phi}\langle x|$: then the expectation value between coherent states is just the Gaussian $\langle \alpha|\delta(x - \hat{x}_\phi)|\alpha\rangle = \sqrt{\frac{2}{\pi}} \exp\{-2\left[x - \mathrm{Re}(\alpha e^{-i\phi})\right]^2\}$).

Before analysing specific matrix representations, let us generalize (10) to the case of non-unit quantum efficiency [4]. Low efficiency detectors in a homodyne scheme simply produce a probability $p_\eta(x, \phi)$ which is a Gaussian convolution of the ideal one $p(x, \phi)$. In terms of the generating functions for the $\hat{x}_\phi$-moments one has

$$\int_{-\infty}^{+\infty} dx\, p_\eta(x, \phi)e^{irx} = \exp(-\frac{1-\eta}{8\eta}r^2) \int_{-\infty}^{+\infty} dx\, p(x, \phi)e^{irx} . \tag{11}$$

Upon substituting (11) into (8) and following the same lines that lead us to (9), one has the sampling formula for low-efficiency detection

$$\hat{\varrho} = \int_0^\pi \frac{d\phi}{\pi} \int_{-\infty}^{+\infty} dx\, p_\eta(x, \phi) K_\eta(x - \hat{x}_\phi) \tag{12}$$

where now the kernel is given by

$$K_\eta(x) = \frac{1}{2}\mathrm{Re} \int_0^{+\infty} dr\, r \exp\left(\frac{1-\eta}{8\eta}r^2 + irx\right) . \tag{13}$$

3. Measurable representations and general bounds

In equation (13) the matrix element $\langle \psi|K_\eta(x - \hat{x}_\phi)|\varphi\rangle$ is bounded if $\langle \psi|e^{-ir\hat{x}_\phi}|\varphi\rangle$ decays faster than $\exp\left[-(1 - \eta)r^2/8\eta\right]$. In order to evaluate the detailed balance of Gaussians in (12) and (13) we introduce the concept of 'resolution' $\varepsilon_\psi^2(\phi)$ of the vector ψ in the $\hat{x}_\phi$-representation

$$|_\phi\langle x|\psi\rangle|^2 \simeq \exp\left[-\frac{x^2}{2\varepsilon_\psi^2(\phi)}\right] \qquad \text{(leading term)} . \tag{14}$$

The resolution $\varepsilon_\psi^2(\phi)$ represent the Gaussian decay length of the probability $|_\phi\langle x|\psi\rangle|^2$ versus x, with the rule that $\varepsilon_\psi^2(\phi) = 0$ and $\varepsilon_\psi^2(\phi) = \infty$ for functions decaying faster and slower than the Gaussian, respectively. Then, let us consider the averaged ('reduced') resolution of the two vectors ψ and φ

$$\frac{1}{\varepsilon^2(\phi)} = \frac{1}{\varepsilon_\psi^2(\phi)} + \frac{1}{\varepsilon_\varphi^2(\phi)} . \tag{15}$$

In terms of $\varepsilon^2(\phi)$ it is easy to state the balance between the decay of $\langle\psi|e^{-ir\hat{x}_\phi}|\varphi\rangle$ and the enhancement of the anti-Gaussian in (13). Taking into account that the Fourier transform is equivalent to a unitary rotation by $\frac{\pi}{2}$ (i.e. $\hat{x}_\phi \to \hat{x}_{\phi+\frac{\pi}{2}}$), one can readily assert that the matrix element $\langle\psi|K(x - \hat{x}_\phi)|\varphi\rangle$ is bounded if the following inequality is satisfied for $\phi \in [0, \pi)$:

$$\eta > \frac{1}{1 + 4\varepsilon^2(\phi)}. \tag{16}$$

Upon maximizing (16) with respect to ϕ we obtain the overall bound

$$\epsilon > \tfrac{1}{2}\sqrt{\eta^{-1} - 1} \tag{17}$$

where

$$\varepsilon^2 = \min_{0\leqslant\phi\leqslant\pi} \{\varepsilon^2(\phi)\}. \tag{18}$$

Hence, in conclusion:

- the matrix element $\langle\psi|\hat{\varrho}|\varphi\rangle$ can be measured if the minimum reduced resolution of vectors ψ and ϕ in the quadrature representations satisfies the bound (17).

In the next section we will consider some particular density matrix representations of interest for applications.

4. Data processing rules for some relevant representations

4.1. Quadrature representation

The resolution is $\varepsilon = 0$ (delta-function): hence it is not possible to measure the density matrix in this representation, even for $\eta = 1$.

4.2. Coherent-state representation

The resolution is $\varepsilon = \frac{1}{2}$: according to (17) the density matrix can be measured for $\eta > \frac{1}{2}$. The data processing rule is given by

$$\langle\alpha|K_\eta(x - \hat{x}_\phi)|\beta\rangle = 2\kappa^2\langle\alpha e^{i\phi}|\beta e^{i\phi}\rangle e^{-2(\kappa x - w_\phi)^2} \Phi\left(-\tfrac{1}{2}, \tfrac{1}{2}; 2(\kappa x - w_\phi)^2\right) \tag{19}$$

with $\kappa = \sqrt{\eta/(2\eta - 1)}$, $w_\phi = \frac{1}{2}(\beta e^{i\phi} + \bar{\alpha}e^{-i\phi})$ and $\Phi(\alpha, \beta; z)$ denoting the degenerate hypergeometric function.

4.3. Number-state representation

The resolution is $\varepsilon = \frac{1}{2}$: the matrix element can be measured for $\eta > \frac{1}{2}$. The data processing rule is given by

$$\langle n|K_\eta(x - \hat{x}_\phi)|n + d\rangle = e^{-id\phi}2\kappa^{d+2}\sqrt{\frac{n!}{(n+d)!}}e^{-\kappa^2 x^2}$$
$$\times \sum_{\nu=0}^{n} \frac{(-)^\nu}{\nu!}\binom{n+d}{n-\nu}(2\nu + d + 1)!\kappa^{2\nu} \operatorname{Re}\left\{(-i)^d D_{-(2\nu+d+2)}(-2i\kappa x)\right\}. \tag{20}$$

In equation (20) $D_\sigma(z)$ denotes the parabolic cylinder function. Notice that the data processing rule does not contain any dimensional truncation of the Hilbert space.

4.4. Squeezed-state representation

The leading term in (14) comes only from the squeezed vacuum (the coherent part just shifts the quadrature). For a squeezed vacuum with squeezing parameter s, the probability of the quadrature $\hat{x}_\phi$ is the Gaussian $|_\phi\langle x|\psi\rangle|^2 = \sqrt{\frac{2s_\phi}{\pi}} \exp(-2s_\phi^2 x^2)$, where $s_\phi = |s^{\frac{1}{2}}\sin\phi - is^{-\frac{1}{2}}\cos\phi|^{-2}$. Hence, the smallest resolution is $\varepsilon = \frac{1}{2}\min(s, s^{-1})$ and the matrix element can be measured for $\eta > [1 + \min(s, s^{-1})]^{-1}$.

5. The number-state representation: statistical errors

Particularly interesting is the possibility of recovering the density matrix in the number-state representation even for quantum efficiency $0.5 < \eta < 1$. In this section we analyse in more detail the analytic form of the kernel (20), also in order to understand the mechanisms producing statistical errors in the measured matrix elements.

In figure 2 the kernel $\langle n|K_\eta(x - \hat{x}_\phi)|n + d\rangle$ is plotted versus x for $\phi = 0$ at different values of η, n and d. One can see that for $\eta = 1$ the range of the plots is essentially constant (between -2 and 2), and increases slowly for large distances $d \gg 1$ from the diagonal. However, for increasing n the kernel oscillates quickly, with a large number of nodes. Fast oscillations make the average of the kernel—hence the measured value $\langle n|\hat{\varrho}|m\rangle$—more sensitive to fluctuations of the random outcomes x of the quadrature, resulting in larger confidence intervals. On the other hand, a constant range makes the errors bounded, so they will saturate at large n's.

For $\eta < 1$ the behaviour of the kernel changes dramatically, with the range increasing versus n, more and more quickly as η approaches the lower bound $\eta = 0.5$. In this case the resulting errors will increase rapidly versus n, and more data will be needed to 'clean out' the noise due to non-unit efficiency.

In figures 3 and 4 the number probability distributions for squeezed states are given from homodyne computer-simulated data: the behaviour of the statistical errors (the shaded area around the horizontal lines) is qualitatively different for $\eta = 1$ (figure 3) and for $\eta = 0.8$ (figure 4). Figure 3 shows the Wheeler–Schleich oscillations [6] of a squeezed state. Figure 4(a) gives the probability for a squeezed vacuum measured for $\eta = 0.8$, whereas figure 3(b) gives the probability for the same data at $\eta = 0.8$, but measured using the kernel with $\eta = 1$: this shows the smearing effect of improper accounting for quantum efficiency. From both figures 3 and 4 it is evident that the present method allows us to recover delicate interference oscillations of non-classical states. The statistical reliability of measured values and confidence intervals have been carefully checked on many Monte Carlo simulations for different kinds of states (see [3]). Here in figures 5 and 6 some checks are reported for coherent states.

6. Wigner function from the density matrix

Despite the fact that the Wigner function cannot be measured directly through homodyne tomography, it can, however, be reconstructed from the measured density matrix in a dimensionally truncated Hilbert space. This can be achieved using the formula

$$W(\alpha, \tilde{\alpha}) = \frac{2}{\pi}\text{Tr}\left[\hat{\varrho} \, e^{2(\alpha a^\dagger - \tilde{\alpha}a)}e^{i\pi a^\dagger a}\right] \tag{21}$$
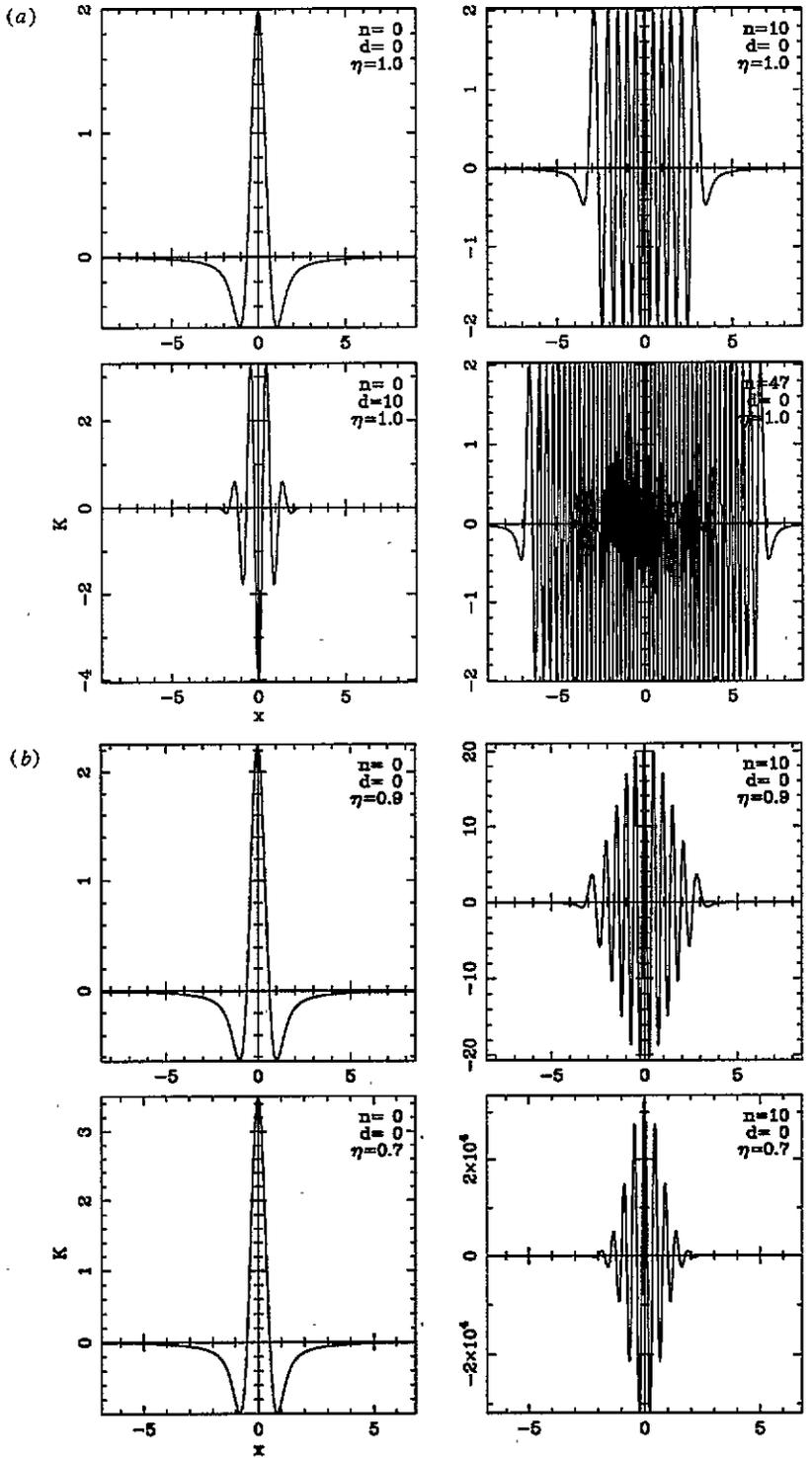
Figure 2. The kernel $\langle n|K_\eta(x - \hat{x}_\phi)|n + d\rangle$. (a) $\eta = 1$; (b) $\eta < 1$.
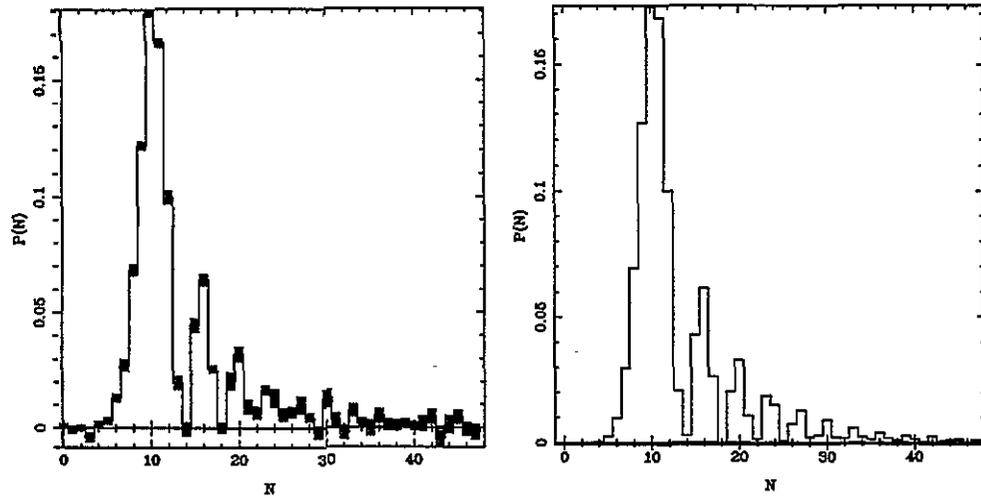
Figure 3. Tomographic reconstruction of the Wheeler–Schleich oscillations of a squeezed state with $\langle \hat{n} \rangle = 13.5125$ and 6.05 squeezing photons. Confidence intervals are represented by the shaded area around the horizontal lines. Detection efficiency is $\eta = 1$. Homodyne data are computer simulated. The plot on the right corresponds to 100 experiments of 2600 phases with 100 data each. On the left only 10 experiments with 260 phases (100 data each) have been used.
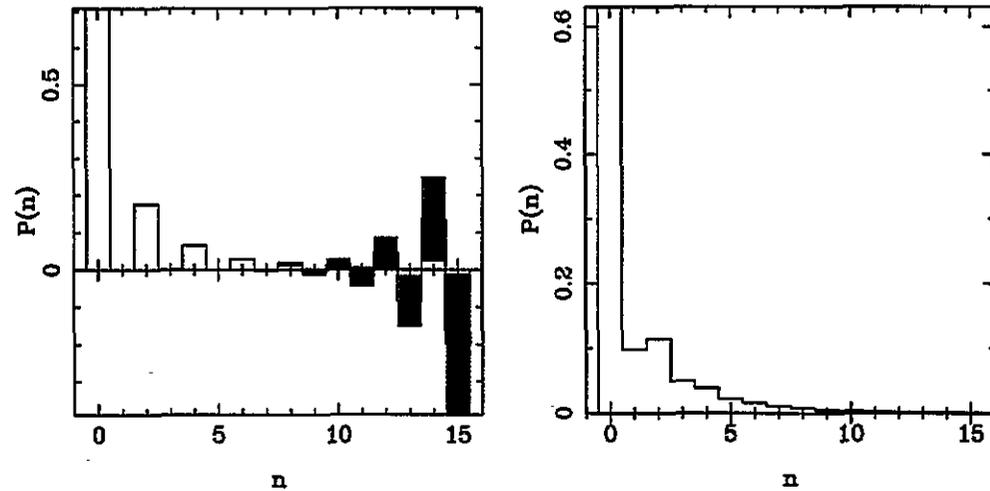
Figure 4. Tomographic reconstruction of the photon-number probability of a squeezed vacuum ($\langle \hat{n} \rangle = 1$) with detection efficiency $\eta = 0.8$. Homodyne data are computer simulated. (Here we averaged over 27 phases using 200 blocks of 5×10^5 data for each phase.) Experimental errors (confidence intervals) are represented by the shaded area around the horizontal lines. (a) Exact reconstruction based on (20). (b) Reconstruction from the same data without taking into account quantum efficiency (namely using (20) for $\eta = 1$).

which in the number representation is rewritten as the Fourier transform

$$W(\alpha, \bar{\alpha}) = \mathrm{Re} \sum_{d=0}^{\infty} e^{\mathrm{i} d \arg(\alpha)} \sum_{n=0}^{\infty} \Lambda(n, d; |\alpha|^2) \varrho_{n,n+d} \qquad (22)$$
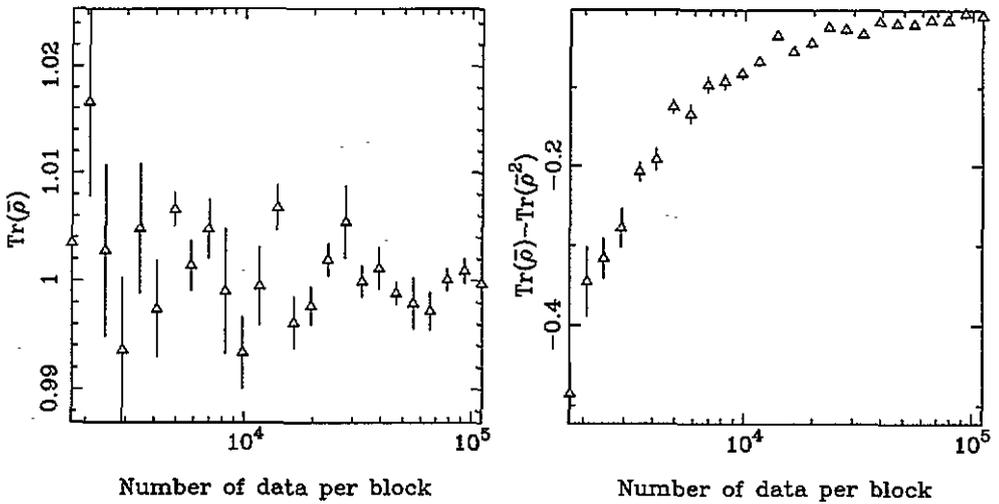
Figure 5. Normalization and mixing of the reconstructed density matrix versus the number data for each experiment (subensemble of data) for a coherent state with $\langle n \rangle = 8$. Detection efficiency is $\eta = 1$. Error bars are estimated on a set of five experiments.
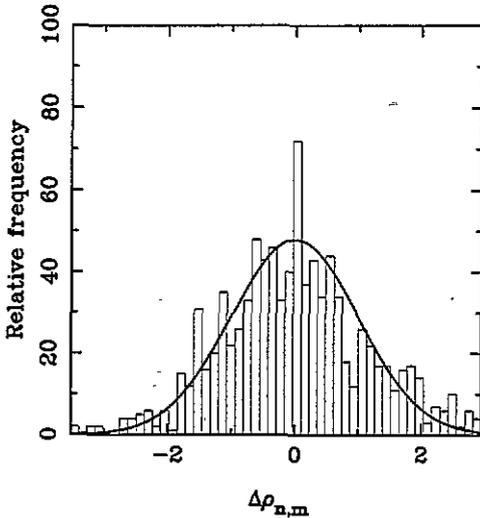
Figure 6. Distribution of normalized deviations from theoretical values $\Delta\varrho_{n,m} \equiv (\bar{\varrho}_{n,m} - \varrho_{n,m})/\varepsilon_{n,m}$ for the first 30×30 matrix elements. Detection efficiency is $\eta = 1$. The quantum state is a coherent one with $\langle n \rangle = 4$. The histogram pertains to 1000 experiments with 27 scanning phases each, and 200 measurements for each phase. A standardized Gaussian curve is superimposed.

with

$$\Lambda(n, d; |\alpha|^2) = (-)^n 2(2 - \delta_{d0})|2\alpha|^d \sqrt{\frac{n!}{(n+d)!}} e^{-2|\alpha|^2} L_n^d(|2\alpha|^2) \qquad (23)$$

and where $L_n^d(x)$ denote Laguerre polynomials. The Hilbert space truncation of the sums in (22) sets a sort of resolution for the reconstruction of $W(\alpha, \bar{\alpha})$. This kind of resolution mostly affects the angular direction (versus $\arg(\alpha)$), whereas radial oscillations come from the Laguerre polynomials as a function of $|\alpha|$. It follows that despite the truncated dimension of the matrix is relatively small, the natural quantum oscillations in the Wigner functions are easily recovered (the truncation of the Hilbert space is set according to normalization checks).
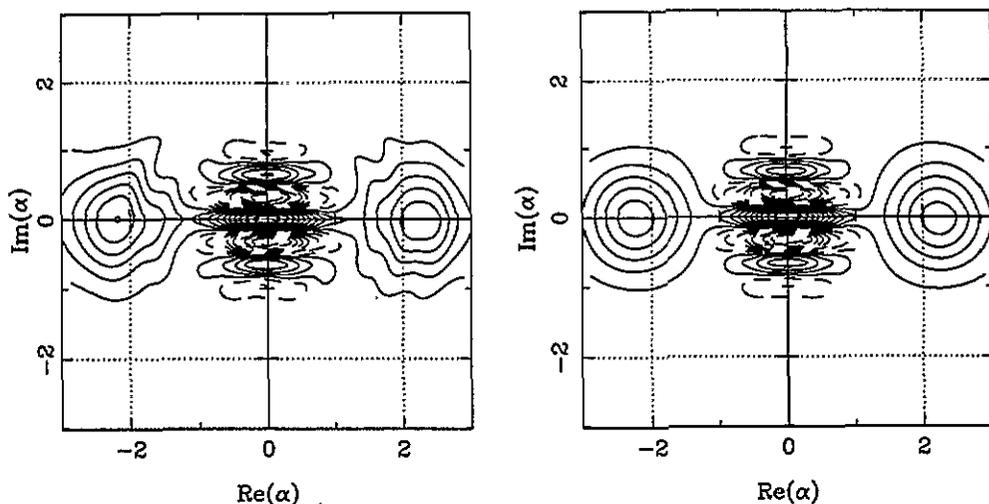
Figure 7. Superposition of two symmetrical coherent states with $\langle n \rangle = 5$ photons each. Wigner functions reconstructed with a tomographically measured density matrix truncated at a maximum of 31 photons. Detection efficiency is $\eta = 1$. 100 experiments and 100 measurements for each phase (left), 10 000 experiments and 1000 measurements for each phase (right). For all plots 27 scanning phases are used.
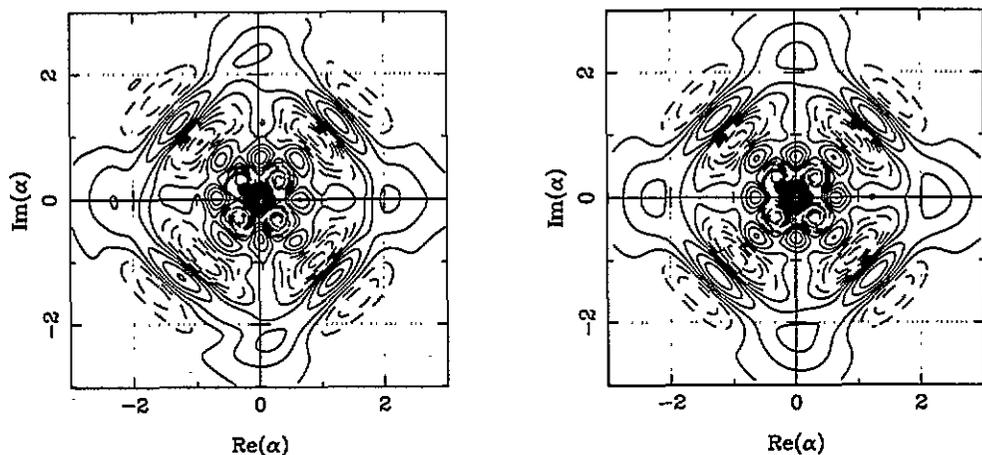
Figure 8. Superposition of four symmetrical coherent states with $\langle n \rangle = 5$ photons each. Wigner functions reconstructed with a tomographically measured density matrix truncated at a maximum of 31 photons, 100 experiments and 100 measurements for each phase (left), 1000 experiments and 1000 measurements for each phase (right). For all plots 27 scanning phases are used. Detection efficiency is $\eta = 1$.

In figures 7 and 8 the Wigner function of Schrödinger cat states are given as reconstructed from homodyne computer-simulated data. It is clear that the old filtered-Radon-transform method [2] would require small cut-offs to recover such Wigner oscillations, thus needing much larger sets of data to be processed.
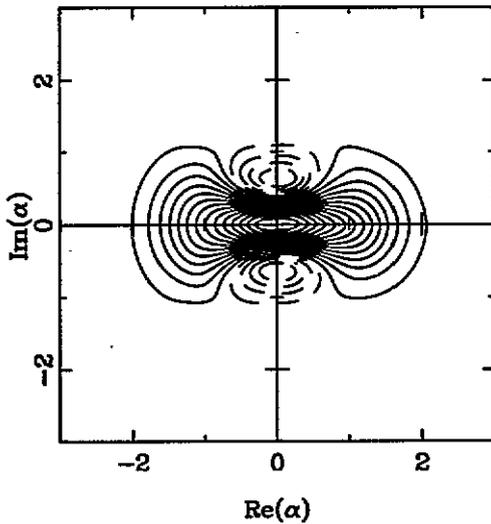
Figure 9. Wigner function of a Schrödinger cat state (superposition of two coherent states with 1 photon each). Reconstruction with $\eta = 0.8$. Here 26 phases are used with 10^8 data each. The truncated dimension of the Hilbert space is 10 photon maximum.

7. 'Classical' and quantum imaging

The reconstruction of the Wigner function from a tomographically measured density matrix can also be regarded as a new tool for imaging. In fact, it is essentially a new kind of regularization of the inverse Radon transform. Corresponding to an image ($\equiv$ density) $W(\alpha, \bar{\alpha})$ in the complex plane—detected from its radial projections $p(x, \phi)$—one has a density matrix $\varrho_{n,m}$ which is no longer positive definite when the image $W(\alpha, \bar{\alpha})$ does not correspond to a genuine Wigner function (namely, that obeys Heisenberg relations for quadratures $\hat{x}_\phi$). The imaging resolution is set by the truncated Hilbert space dimension $d_{\mathcal{H}}$, and the image is 'compressed' into the truncated density matrix $\{\varrho_{n,m}\}_{n,m=0}^{d_{\mathcal{H}}-1}$. The distance between the 'true' and the 'reconstructed' images is given by

$$\int d^2\alpha |\Delta W(\alpha, \bar{\alpha})|^2 = \text{Tr}(\Delta\hat{\varrho})^2 \tag{24}$$

which is just the Hilbert distance between the true and the reconstructed density matrix. It is clear that the method can be used for both deterministic $p(x, \phi)$ (namely, analytically given) and for data random distributed according to $p(x, \phi)$. However, the method is particularly convenient in the latter case, whereas in the former it is just an image compression tool.

A typical situation for imaging from random data can be depicted as follows. Imagine equipment for x-ray tomography using very low fluxes. Instead of collecting the profiles $p(x, \phi)$ of radial x-rays for various ϕ's (then evaluating the filtered backprojection) one collects the locations $\{x\}_\phi$ of the (not-too-many) photons along the line perpendicular to the ϕ-direction. Then, from the locations $\{x\}_\phi$ one obtains the density matrix $\varrho_{n,m}$ using (20), and finally with (22) one reconstructs the image $W(\alpha, \bar{\alpha})$.

In figure 10 the image of the letter 'a' is reconstructed from simulated radial data. It is evident that the image is 'classical' (it does not correspond to a genuine quantum Wigner function), because the relevant details of the image are much smaller than the Planck cell—a unit square in this plot.
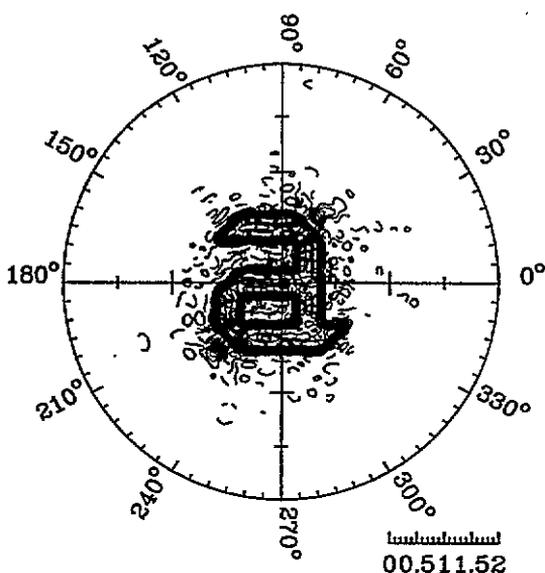
Figure 10. Imaging of the letter 'a': the data processing rule in (20) and (22) is used as a new kind of regularization of the inverse Radon transform. Radial data are computer simulated (10 experiments with 100 phases, 1000 data each).

8. Conclusions

The method described in this paper is a genuine measurement of the density matrix. Data processing does not rely on *a priori* statistical hypotheses, and the analytic form of the processing is derived theoretically without approximations. The statistical reliability of confidence intervals is based on the central-limit theorem, with excellent checks on Monte Carlo simulations. We have seen that some matrix representations cannot be measured—the quadrature and the Wigner—whereas others can—the number and the coherent representations for $\eta > \frac{1}{2}$. On the basis of computer-simulated experiments we have seen how delicate quantum oscillations of probabilities can be detected experimentally, also overcoming the smearing effect of non-unit efficiency. Finally, I showed that the method itself can be used as a new imaging and/or compression algorithm for conventional tomography, with the greatest advantage being in the presence of random data.

References

[1] Vogel K and Risken H 1989 *Phys. Rev.* A **40** 2847
[2] Smithey D T, Beck M, Raymer M G and Faridani A 1993 *Phys. Rev. Lett.* **70** 1244
[3] D'Ariano G M, Macchiavello C and Paris M G A 1994 *Phys. Rev.* A **50** 4298; 1994 *Phys. Lett.* **195A** 31
[4] D'Ariano G M, Leonhardt U and Paul H *Phys. Rev. Lett.* submitted
    See also Smithey D T, Beck M, Cooper J and Raymer M G 1993 *Phys. Rev.* A **48** 3159 and references therein
[5] D'Ariano G M, Macchiavello C and Paris M G A (unpublished)
[6] Schleich W and Wheeler J A 1987 *Nature* **326** 574